Design of a low-frequency impedance measurement system applicable to LV grids in live conditions

Andrea Mariscotti
DITEN
University of Genova
Genova, Italy
0000-0002-0096-7305

***Abstract*—The design of an impedance measurement system is discussed for application in low-voltage power grids in operation, addressing the presence of the grid voltage. A shunt injection arrangement is preferred, relying then on the measurement of the port voltage and current. A Twin-T passive filter is designed to buffer the isolating injecting transformer, suppressing the $50\,\mathrm{Hz}$ fundamental and avoiding excessive magnetizing current and voltage the signal generator connected to the secondary side. Before construction, the system has been simulated and parameters values optimized, showing good performance even with very large-power grids with impedance Z_g of tens of $\mathrm{m\Omega}$. Z_g estimate uncertainty is $< 1\,\%$ at coverage factor $k = 1$.**

***Index Terms*—current probe, impedance measurement, power grids, uncertainty, voltage probe.**

I. Introduction

Information on the impedance value of an electric grid is useful from several viewpoints. Knowledge of grid impedance (Z_g) helps in grid planning and operation, control and protection, that are all processes taking place at the fundamental frequency and in general at low frequency (LF). Distortion prediction and mitigation is another key point and we have observed a transition of studies and assessment from the traditional harmonic range to higher frequency, i.e. the supra-harmonic (SH) range [1], [2]. It is well known that radio-frequency conducted emissions and the efficacy of filters strongly depend on grid and load impedance [3]. This is even more important in the harmonic and SH intervals, where larger impedance variability is expected, not only for the frequent connection and disconnection of sources and loads, but also for various resonance conditions [4].

Z_g measurement methods in live conditions may be classified from different viewpoints, e.g. frequency- and time-domain processing (so focusing on sine-waves at variable frequency or step-like or impulse-like signals, including grid transients) [5]. In general the preferred classification is between active and passive methods:

- Active methods inject an excitation signal to test Z_g by either measuring directly voltage and current (voltamperometric methods) or direct and reflected components (methods using Vector Network Analyser, VNA). The excitation may be tones or a swept sine in a frequency-domain perspective, or impulsive or step-like signals in a time-domain perspective.
  - VNA-based methods, using 2-probe configuration [6], perform better in the high-frequency range, and may suffer from non-ideality of the used probes (saturation), complex wiring for on-site use and limited VNA performance approaching LF [7], [8];
  - voltamperometric methods, where a test signal is applied to the measuring port and voltage and current are separately measured; this method can be used at high frequency [9], [10], but is suitable also for the LF interval (from nearly DC up to $9\,\mathrm{kHz}$).
- Passive methods exploit instead excitation signals occurring during operation, passively listening to the grid. These methods are particularly suitable for electric grids with large power levels and/or high voltage, where external excitation would be impractical. A common approach is to use a multitude of measuring points by means of phasor measurement units [11], which, however, are hardly applicable at the distribution level and pose a significant accuracy requirement for voltage and current transformers, besides a tight time reference [12].

Methods are in general best applicable in out-of-service conditions, not only for a mere matter of electrical safety, but also to achieve better dynamic range and to reduce noise and non-linearity problems. This rules out also any pre-existing voltages in the measured grid. In reality the contribution of modern power converters to the variability of Z_g is crucial and this can be assessed only in live and full operating conditions. This entails the mentioned issues of non-linearity and sensors robustness, besides the presence of large signals at the mains frequency (assumed for simplicity $50\,\mathrm{Hz}$), causing issues of dynamic range and worsening sensitivity and vertical resolution. This latter point represents a challenging point of novelty with respect to other solutions, operating always beyond the fundamental frequency [13], [14].

The entire LF interval is considered instead with particular attention as part of the Met4EVCS Project [15], studying among other points the influence of Z_g on electric vehicle charging stations and viceversa.

This paper thus focuses on the design of a LF Impedance Measuring System (IMS), solving problems related to live con-

ditions, signal-to-noise ratio at the test port (the Internal Point of Coupling, IPC) with respect to dynamic range requirements to improve vertical resolution, with less demanding injected current amplitude for large power grids. The paper develops from a discussion of requirements in Section II, to the design of the most relevant IMS components, bringing in the novelty of the proposed system (Section III). Section IV then focuses on selected hardware and instrumentation and provides the uncertainty budget. Feasibility and performance are demonstrated by means of simulation; tests on the prototype will be carried out in summer for use in the mentioned EU-funded project.

II. Problem requirements and constraints

Application requirements and constraints are considered, examining published alternative solutions, substantiating the design choices and providing discussion of the state of the art for the measurement of LF Z_g. The LF range spans from almost DC to the largest harmonic frequency (2 kHz) or the lowest frequency of the RF conducted emissions, 9 kHz.

The expected Z_g values may range from tens of mΩ (large-power grid with a 1 MVA transformer) up to hundreds of Ω at resonances.

A. Existing realizations

Voltamperometric active methods inject a test current I_t superposed to the normal operating current, measuring the grid voltage and current variation δV_g and δI_g and estimating Z_g as $= \delta V_g/\delta I_g$) [16]. Published methods consist of:

- series current injection by current transformer (CT), e.g. of the clamp-on type, as for earthing resistance measurements, with injected current limited to about 200 mA in a low-resistance circuit (the earthing circuit) [17];
- shunt injection using power amplifiers [18] or suitably controlled inverters [19];
  - it is underlined that the former [18] was used for measurements well above the fundamental frequency (starting at 1 kHz, filtering out the fundamental and its highest harmonics;
  - solutions using inverters instead can operate around the fundamental, but their ratings are similar to grid loads and quite expensive, and feature the intrinsic limitation of semiconductors switching speed, with maximum applied frequency up to 10 kHz.

B. Proposed large bandwidth solution

Coupling of the test signal I_t may be implemented by a clamp-on probe (series injection) or by direct injection at an accessible node (shunt injection), as shown in Fig. 1.

A sweeping excitation signal is injected into the Internal Point of Coupling (IPC) port: the grid on the left is characterized by Z_g and the load on the right by Z_l quantities.

The injection geometry is in "derived mode" (so through a third branch sharing the IPC as common node). The branched injection allows to distinguish the left and right hand side sections, by measuring the respective currents. A series injection,

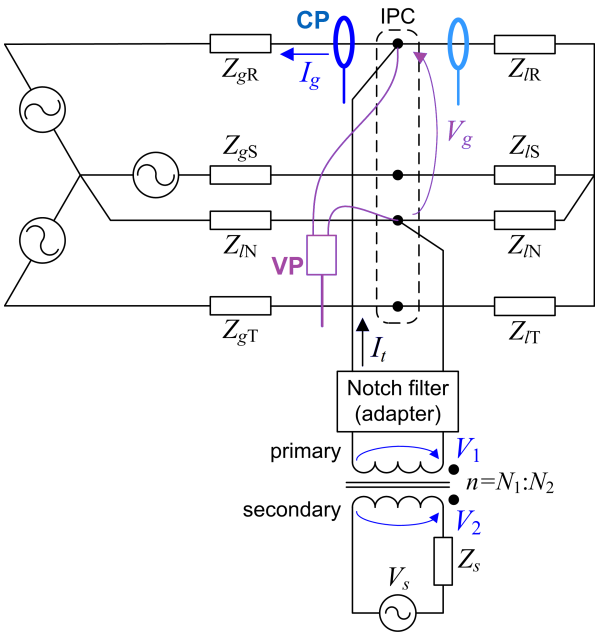

Fig. 1. IMS schematic for a hypothetical 3-ph. grid with neutral for the measurement of Z_g between phase R and N. Current probe (CP) measures the current I_g into the IPC (the other CP in light blue is optional); the voltage probe (VP) measures V_g at the IPC port.

instead, would have made grid and load not separable. I_g and I_l may be measured with LF clamp-on probes.

Although clamp-on coupling seems less invasive, as it does not modify at all the system configuration, the ability of injecting a suitable test current intensity is compromised as soon as Z_g is above some tens of Ω, reducing drastically as soon as the system approaches high-impedance regions. Clamp-on probes then have non-negligible physical size that requires anyway some modification, like stripping cable sheath to separate the internal conductors, or use of short wire patches to allow one or a few turns around the clamp. A preliminary check with the clamp-on probes equipping the Chauvin Arnoux mod. 6471 meter [17] has shown that injected current in a simulated grid is limited to about a few tens of mA approaching overloading and only above 100 Hz.

Another drawback is that clamp-on coupling applies a series injection allowing the determination only of Z_g and Z_l combined. The use of shunt injection at the coupling port, conversely, allows separating the current flowing into the two directions, leading to separate evaluation of Z_g and Z_l.

The proposed solution consists of a direct signal injection by a coupling transformer, driven by a power amplifier. Being the selected band covering all LF components including the fundamental and its harmonics, the unavoidable coupling and consequential rating of components is favourably reduced by using a notch filter for the 50 Hz fundamental (adjustable to 60 Hz). The notch filter has two benefits: reduction of power dissipation on downstream devices and reduction of the magnetizing current flowing into the transformer, allowing using transformers with lower nominal voltage. Such filter is

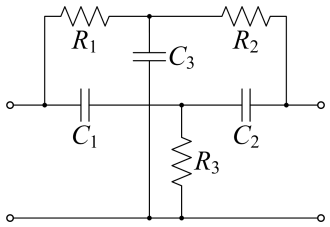

Fig. 2. Twin-T notch filter schematic.

directly connected to the grid and the best architecture is the twin-T notch filter shown in Fig. 2.

For grids with higher nominal voltage, a 230 V transformer may still be used, provided that magnetizing current is not excessive and voltage insulation ratings are not approached during normal use.

For the test signal generation and its coupling, what is the required I_t intensity? The $Z_{g,\text{min}}$ value implies a corresponding $I_{t,\text{max}}$, once the minimum measurable port voltage $V_{t,\text{min}}$ is considered. This quantity is determined not only by the instrumentation, but also by the existing noise in the LF interval. Assuming $V_{t,\text{min}} = 1\,\text{mV}$, the resulting $I_{t,\text{max}} = 100\,\text{mA}$, as most of earth resistance and fault-loop impedance testers [17].

Considering the V_t measurement, typical differential voltage probe (VP) noise is in the order of some mV to a tenth of mV [20]–[22], measured as broadband rms and reduced by almost an order of magnitude if measured in the LF interval only.

An important point to consider is the possible VP non-linearity in the presence of a large fundamental signal. This is never documented to author's knowledge, but we can say that if occurs, it will affect only the fundamental harmonics, that, to stay on the safe side, may be discarded from the pool of measured frequencies during post-processing. Anyway this is an interesting point that is part of the activities in the Met4EVCS Project [15].

The data acquisition system (DAS), instead, suffers from the inability of rejecting the fundamental that determines thus the required full scale. Also in this case an improvement comes from the use of a downstream notch filter.

Assuming a VP constant attenuation (100 for the Testec SI-9010), we can reason on the values at the injecting port to fulfil requirements of detectability and signal-to-noise ratio at the DAS and feasibility for current and power rating. This is summarized below, focusing on some devices and items of equipment for exemplification purposes.

- the $400\,\text{V}$ maximum nominal voltage sets the DAS full scale; the notch filter can reduce it down to about $15\,\text{V}$, comparable to the largest harmonic distortion components; the VP attenuation (100 for the Testec SI-9010) transfers this to the DAS as $200\,\text{mVpk}$;
- the 16-bit DAS has a quantization noise floor in the order of $1.8\,\mu\text{Vrms}$ to $4.4\,\mu\text{Vrms}$, giving $0.4\,\text{mVrms}$ over the entire $10\,\text{kHz}$ bandwidth; this value is still smaller than the assumed VP output noise, that for the Testec SI-9010 amounts to $0.9\,\text{mVrms}$; assuming a resolution frequency of $10\,\text{Hz}$ the noise in each frequency bin amounts to $0.03\,\text{mVrms}$, or $3\,\text{mVrms}$ at the IPC (grid side), that is an estimate of the IMS sensitivity;
- the assumed nominal $I_t = 100\,\text{mArms}$ causes the IPC voltage to stay above the sensitivity for $Z_g > 30\,\text{m}\Omega$; larger test current intensity is necessary for extremely stiff grids; in a real-world scenario $30\,\text{m}\Omega$ is the impedance of a $630\,\text{kVA}$ MV/LV transformer accounting for some meters of cable;
- assuming an overestimating $I_{t,\text{max}} = 0.5\,\text{Arms}$ in a $400\,\text{Vrms}$ phase-to-phase configuration, leads to $200\,\text{VA}$ of rating for the step-up transformer.

III. IMS DESIGN AND SIZING

A. Twin-T notch filter

This is a well-known notch filter architecture and probably the only suitable circuit for passive implementation. Active implementations may instead rely on alternative schemes, like the Fliege, Wien, etc.

The Twin-T circuit has a known optimized form where the transversal components R_3 and C_3 are equal to $R/2$ and $2C$, respectively, having the series components equal to R and C. The general transfer function (neglecting source and load impedances) is a third-order polynomial (having 3 capacitors), that simplifies to a second-order one with the parameters choice above (zero-pole cancellation). Under such conditions the notch frequency can be determined as:

$$f_0 = \frac{1}{2\pi RC} \tag{1}$$

Values in the Twin-T notch filter were determined trading off power dissipation, reduction of the magnetizing current, avoiding excessive impedance at other frequencies not to limit the injected current amplitude. A first version was identified (version 1) using $C = 4.7\,\mu\text{F}$, available as the largest value for safety capacitors with the $400\,\text{Vrms}$ voltage rating, and $R = 680\,\Omega$ power resistors (the exact value being $677.3\,\Omega$, but not including source and load resistance, so achieved practically by fine tuning on the final implementation).

A second version (version 2) of the Twin-T was also considered, where a factor of 2 is applied, reducing the resistor values to one half and doubling the capacitors values with the objective of increasing the injected current amplitude.

B. Transformer and sourcing impedance

The transformer was selected with configurable primary and secondary windings, both split into two halves ($2 \times 115\,\text{V}/2 \times 24\,\text{V}$) with a rated power of $200\,\text{VA}$, to limit its weight, and relying on the fact that power rating is specified for continuous operation at the highest operating temperature.

The primary inductance of the two series-connected windings is about $0.9\,\text{H}$, or $300\,\Omega$ at $50\,\text{Hz}$. As anticipated, the considered Twin-T filter configurations have been the $C = 4.7\,\mu\text{F}\&R = 680\,\Omega$ ("version 1") and the $C = 9.4\,\mu\text{F}\&R = 340\,\Omega$ ("version 2"), the latter with a slightly larger dissipation, but allowing a higher injected current (almost double) for the same test signal amplitude.

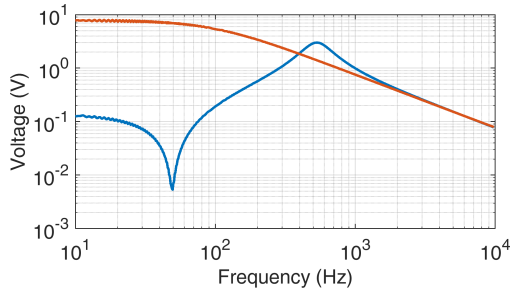

Fig. 3. Voltage coupled on the signal generator with 100 V grid voltage with (blue) and without (orange) notch filter.

Dissipation values in W are shown in Table I. They were calculated using a maximum fundamental amplitude with worst-case large distortion for each frequency interval, i.e. at the fundamental, at the first low-order harmonics, and then up to 3 kHz. The preponderant dissipation is at the fundamental, as expected, with much smaller value at the harmonic frequencies, fluctuating as the current changes path through the twin-T circuit. The highest dissipation is for R_1 and amount to 110 W.

TABLE I. Dissipation for the two twin-T filter versions.

Freq. (Hz)	Voltage (Vrms)	Twin-T version 1			Twin-T version 2		
		P_{R_1}	P_{R_2}	P_{R_3}	P_{R_1}	P_{R_2}	P_{R_3}
50	230	89.1	17.7	35.7	97.5	19.4	39.0
100	30	1.09	0.12	0.49	2.12	0.39	0.97
150	30	1.17	0.13	0.55	2.25	0.46	1.19
250	15	0.30	0.06	0.16	0.58	0.23	0.44
350	15	0.30	0.10	0.20	0.59	0.39	0.64
450	15	0.30	0.17	0.26	0.60	0.56	0.87
550	15	0.30	0.27	0.37	0.61	0.70	1.09
650	15	0.31	0.38	0.49	0.62	0.80	1.25
750	15	0.31	0.47	0.62	0.63	0.85	1.36
1500	15	0.33	0.47	0.78	0.66	0.78	1.42
2250	15	0.33	0.40	0.72	0.66	0.72	1.38
2250	15	0.33	0.37	0.70	0.66	0.70	1.36

The effectiveness of the notch filter is verified by simulating the system with and without it, assuming a flat 100 V grid voltage at all frequencies and looking at the voltage coupled on the signal generator. Such amplitude was chosen because much closer to actual values, providing direct indication of the expected signal magnitude. The results are shown in Fig. 3: the 50 Hz is suppressed by almost 3 orders of magnitude and the largest harmonics by approximately a factor of 3, having identical behaviour above 1 kHz.

The overall behaviour is verified by simulating the injection of the test signal into a grid of variable impedance Z_g, made of a series connection of resistance R_g and inductance L_g. Fig. 4 shows the injected current into the grid I_g, the IPC voltage V_g, the primary voltage V_1 and the secondary voltage V_2 for $R_s = 1\,\Omega$. A wide range of grid parameters is swept, from large resistive ($R_g = 200\,\Omega$) to moderate resistive ($R_g = 2\,\Omega$), to very low values typical of a large short-circuit power ratio grid ($R_g = 0.02\,\Omega$ and $L_g = 20\,\mu$H).

The results for 1 Ω (Fig. 4) demonstrate that I_g maintains

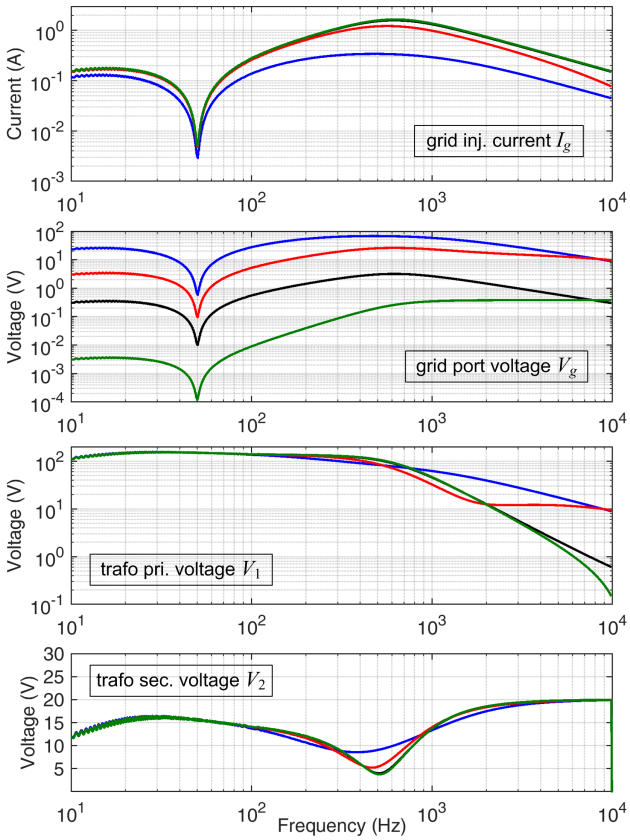

Fig. 4. Voltage and current levels over the 10 Hz to 10 000 Hz interval: black ($R_g = 2\,\Omega$), blue ($R_g = 200\,\Omega$), red ($R_g = 20\,\Omega$ and $L_g = 2$ mH) and green ($R_g = 0.02\,\Omega$ and $L_g = 20\,\mu$H). Test signal generation with $R_s = 1\,\Omega$.

a level of 100 mA to 200 mA with the desired notch around 50 Hz, characterized by only 5 mA at 50 Hz and about 40 mA at 40 and 60 Hz.

A slightly more uniform current injection can be achieved increasing the generator resistance at the expense of a lower injected current (about 30 mA for 10 Ω). One may wonder if some equalization with reduction of current at high frequency may be achieved by modifying the generator impedance. Simulations were carried out with an inductor of 0.1 mH to 10 mH added in series to $R_s = 0.1\,\Omega$, and the results are shown in Fig. 5. This maximizes the current injected at LF (200 mA applying a test signal of 20 V) and reduces the high-frequency current, keeping it below about 1 A with the series inductance > 1 mH.

IV. LF IMS Architecture and Uncertainty

A. Implementation

The blocks discussed and designed in the previous section are assembled to form the three functions of the IMS: test current injection, port voltage measurement and branch current measurement, all connected to the DAS.

The IPC voltage can then be measured by using an isolated voltage probe and the Testec SI 9010 was selected for a

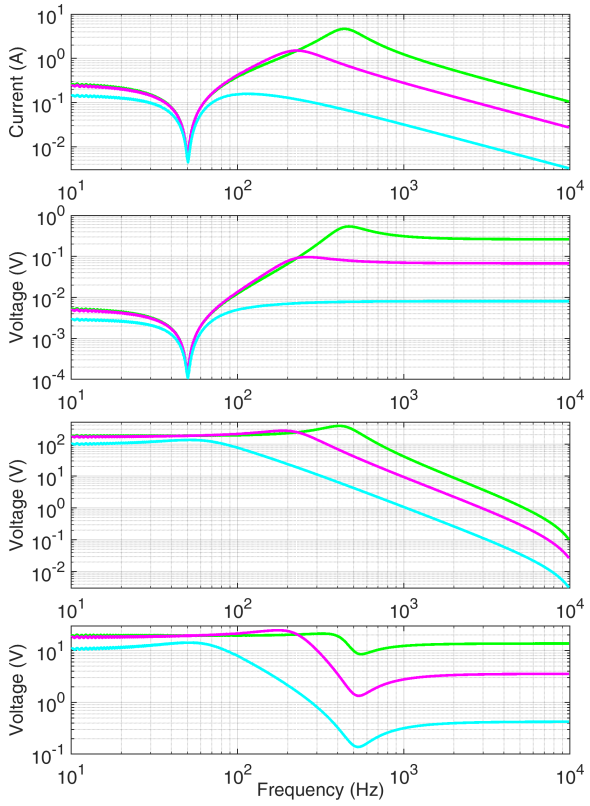

Fig. 5. Voltage and current levels over the 10 Hz to 10 000 Hz interval with the most challenging grid impedance of $Z_g = 20\,\mathrm{m\Omega} + 40\,\mu\mathrm{H}$: green ($Z_s = 0.1\,\Omega + 0.1\,\mathrm{mH}$), magenta ($Z_s = 0.1\,\Omega + 1\,\mathrm{mH}$) and cyan ($Z_s = 0.1\,\Omega + 10\,\mathrm{mH}$).

matter of availability and very low internal noise, besides the abundant insulation level.

The current probes used for the measurement of I_g and I_l are from the CA 6471 instrument, but they may be replaced by Rogowski coils or closed fluxgate sensors, with different uncertainty contributions.

The active twin-T filter is used to reject the incoming 50 Hz from the voltage and current probes. The values are optimized selecting available resistors values (26.1 kΩ) leading to a capacitance of 122 nF, obtained by paralleling two standard values. The so obtained notch frequency is 49.983 Hz: $C_{21} = C_{22} = C_{23}/2 = 122\,\mathrm{nF}$ and $R_{21} = R_{22} = 2 \times R_{23} = 26.1\,\mathrm{k\Omega}$. Such resistors can be found with 0.1 % accuracy and $10\,\mathrm{ppm/°C}$ temperature coefficient. Capacitors are 1 % or 2 % and the worst-case temperature coefficient is $30\,\mathrm{ppm/°C}$, although much smaller at room temperature up to about 45 °C.

B. Uncertainty budget

The discussed coupling method through the step-up transformer and Twin-T notch filter does not contribute to uncertainty, as all quantities that define the grid impedance are separately measured. Rather, correct sizing and rating allows a more ideal behaviour, with a sufficiently flat test current and acceptable dissipation and self heating.

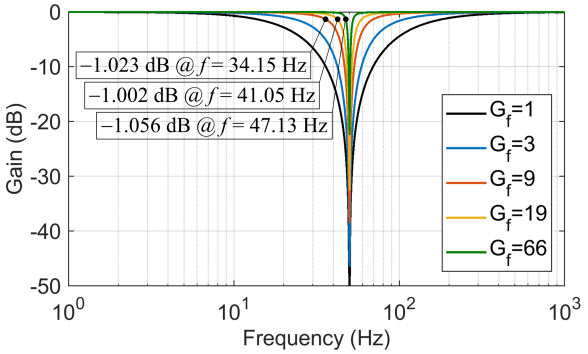

Fig. 6. Active Twin-T notch filter FR for different gain G_f values.

The grid impedance Z_g, determined as the ration of the IPC voltage V_g and grid current I_g, has thus a straightforward uncertainty expression:

$$u\{Z_g\} = \sqrt{(u\{V_g\})^2 + (u\{I_g\})^2} \tag{2}$$

The factors contributing to the uncertainty of V_g and I_g are the uncertainty associated to the respective probes and the two DAS channels, including the signal notch filters before the DAS channels.

The current probe (CA-C180) has a declared accuracy of ±0.5 % with a phase shift of less than 1 deg at 50 Hz. In addition other two terms of uncertainty are the influence of adjacent conductors (declared less than 0.05 % at 50 Hz) and of conductor positioning within the probe jaws (declared less than 0.1 % up to 400 Hz). The voltage probe (Si-9010) has a declared accuracy of ±2 % [22]. This is a conservative statement that also lacks the phase shift characterization: an ad-hoc calibration should possibly reduce it to less than 1 %.

The DAS channels have the following contribution:

- The quantization noise term can be theoretically estimated at 0.02 % for a 12-bit system with a full scale signal; if the applied signal is only 1 % of the full scale, the contribution becomes 2 % relative, larger than that of probes. The presence of the fundamental forces the selection of a large range; this can be avoided only with an active notch filter. This does not occur when measuring only the SH range, as all probes have high-pass behaviour.
- The vertical amplitude accuracy (aka "DC accuracy") is better than 1 % [23], but can be reduced drastically by individual calibration; the remaining temperature dependency and non-linearity terms are not better documented.

The active notch twin-T filter (designed as in [24]) is characterized by the capacitors accuracy in the first place (2 %), but individual calibration can reduce it to the used instrument uncertainty plus the contribution of the temperature variability, < 300 ppm for ±10 °C of variation.

Flatness of its frequency response (FR) can be corrected after calibration, but it helps having an almost ideal channel response. The results of PSpice simulations are shown in Fig. 6, for a range of values of the feedback gain G_f and, as a consequence, of the factor of merit.

Assuming all accuracy terms with a uniform distribution of the error and the use of the notch filter for fundamental suppression, the resulting uncertainty for Z_g is less than $\pm 1\,\%$ with unitary coverage factor (relying on what declared in the respective datasheets).

V. Conclusion

The design of a LF IMS was discussed, focusing on feasibility for rating, power dissipation, dynamic range and resolution, as "live conditions" implies the presence of the grid voltage causing the following problems: electrical safety issues, saturation of the coupling transformer at highest voltages, dissipation and unfavourable dynamic range at the DAS. The system was kept simple, using a coupling transformer to inject into the IPC, buffered by a $50\,\mathrm{Hz}$ passive twin-T notch filter.

The effectiveness of the passive notch filter has been demonstrated, showing a significant reduction of the fundamental (almost 3 orders of magnitude) and first harmonics, reducing both chances of saturation of the transformer if used at higher nominal voltages and the flow of large fundamental current at the secondary and into the signal generator.

The grid impedance is estimated by a simple IPC voltage/current ratio and its uncertainty $u\{Z_g\}$ is derived from that of the measuring probes and DAS. Without special corrections and ad-hoc calibrations, $u\{Z_g\}$ was estimated better than $1\,\%$ with $k = 1$ coverage factor if suppressing the fundamental large swing. The dynamic range may be in fact significantly improved by adding an active notch filter on each channel, allowing a reduction of the full scale by more than an order of magnitude and improved sensitivity.

The proposed IMS can be applied to online real-time measurement of the grid impedance during operation as the intensity of the injected signal can be adapted to avoid interference. The system is flexible for the choice of the voltage and current probes to adapt to the particular characteristics of the grid and loads.

This IMS addresses one of the requirements for impedance measurement in the DC to $9\,\mathrm{kHz}$ frequency interval of the Met4EVCS project [15]. After its construction in summer 2025, it will be extensively used in the planned test campaigns.

Acknowledgment

The project 23IND06 Met4EVCS receives funding from the European Partnership on Metrology, co-financed from the European Union's Horizon Europe Research and Innovation Programme and by the Participating States.

References

[1] A. Mariscotti, "Harmonic and supraharmonic emissions of plug-in electric vehicle chargers," *Smart Cities*, vol. 5, no. 2, pp. 496–521, apr 2022.

[2] J. Sutaria, S. Rönnberg, and A. Espín-Delgado, "Factors influencing the induced primary emission and induced secondary emission in the frequency range of 2 to 150 kHz," *Electric Power Systems Research*, vol. 224, p. 109725, Nov. 2023.

[3] K.-R. Li, K.-Y. See, and R. M. Sooriya Bandara, "Impact analysis of conducted emission measurement without lisn," *IEEE Transactions on Electromagnetic Compatibility*, vol. 58, no. 3, pp. 776–783, Jun. 2016.

[4] S. Bhagat, A. Mariscotti, M. Simonazzi, and L. Sandrolini, "Variability of conducted emissions of EV chargers due to mutual effects on a DC grid," in *2023 International Symposium on Electromagnetic Compatibility – EMC Europe*. IEEE, Sep. 2023.

[5] M. K. De Meerendre, E. Prieto-Araujo, K. H. Ahmed, O. Gomis-Bellmunt, L. Xu, and A. Egea-Alvarez, "Review of local network impedance estimation techniques," *IEEE Access*, vol. 8, pp. 213 647–213 661, 2020.

[6] V. Tarateeraseth, B. Hu, K. Y. See, and F. Canavero, "Accurate extraction of noise source impedance of an SMPS under operating conditions," *IEEE Transactions on Power Electronics*, vol. 25, no. 1, pp. 111–117, Jan. 2010.

[7] S. Büyük, A. Mariscotti, K. Štibernik, O. Şen, and M. Wojciechowski, "A portable VNA-based system for grid impedance measurements," in *2024 International Symposium on Electromagnetic Compatibility – EMC Europe*. IEEE, Sep. 2024, pp. 464–469.

[8] A. Mariscotti and M. Mayerhofer, "Testing non-linearity and saturation of a RF current probe," in *EMC Europe*, Paris, France, 2025.

[9] I. Fernández, D. de la Vega, D. Roggo, R. Stiegler, L. Capponi, I. Angulo, J. Meyer, and A. Arrinda, "Comparison of measurement methods of lv grid access impedance in the frequency range assigned to nb-plc technologies," *Electronics*, vol. 8, no. 10, p. 1155, Oct. 2019.

[10] I. Fernández, A. Gallarreta, J. González-Ramos, P. Wright, D. de la Vega, I. Angulo, and A. Arrinda, "Measurement system of the mean and sub-cycle LV grid access impedance from 20 kHz to 10 MHz," *IEEE Transactions on Power Delivery*, vol. 38, no. 3, pp. 2204–2212, Jun. 2023.

[11] M. Asprou, E. Kyriakides, and M. M. Albu, "Uncertainty bounds of transmission line parameters estimated from synchronized measurements," *IEEE Transactions on Instrumentation and Measurement*, vol. 68, no. 8, pp. 2808–2818, Aug. 2019.

[12] A. Mingotti, L. Peretto, and R. Tinarelli, "A novel equivalent power network impedance approach for assessing the time reference in asynchronous measurements," in *IEEE International Instrumentation and Measurement Technology Conference (I2MTC)*. IEEE, May 2017, pp. 1–6.

[13] J. Xie, Y. X. Feng, and N. Krap, "Network impedance measurements for three-phase high-voltage power systems," in *2010 Asia-Pacific Power and Energy Engineering Conference*. IEEE, 2010, pp. 1–5.

[14] R. Stiegler, J. Meyer, P. Schegner, and D. Chakravorty, "Measurement of network harmonic impedance in presence of electronic equipment," in *2015 IEEE International Workshop on Applied Measurements for Power Systems (AMPS)*. IEEE, Sep. 2015, pp. 1–6.

[15] 23IND06 Met4EVCS Project, "Metrology for electric vehicle charging systems," https://www.vsl.nl/en/met4evcs/ (available online, last accessed on May 15, 2025), 2024.

[16] D. Borkowski, "A new method for noninvasive measurement of grid harmonic impedance with data selection: Method for noninvasive measurement," *International Transactions on Electrical Energy Systems*, vol. 25, no. 12, pp. 3772–3791, Mar. 2015.

[17] Chauvin Arnoux, "CA6471 User Manual, 100331 v12," 2015.

[18] A. A. Girgis and R. B. McManis, "Frequency domain techniques for modeling distribution or transmission networks using capacitor switching induced transients," *IEEE Power Engineering Review*, vol. 9, no. 7, pp. 74–75, 1989.

[19] H. Hu, P. Pan, Y. Song, and Z. He, "A novel controlled frequency band impedance measurement approach for single-phase railway traction power system," *IEEE Transactions on Industrial Electronics*, vol. 67, no. 1, pp. 244–253, Jan. 2020.

[20] Hameg, "HZ probes datasheet," https://www.tequipment.net/Hameg/HZ115/ (available online, last access on 13-05-2025), 2024.

[21] Testec, "SI-9002 differential voltage probe," https://testec.de/en/products/differential-probes.html (available online, visited on 25-05-2025), 2016.

[22] ——, "SI-9010 differential voltage probe," https://testec.de/en/products/differential-probes.html (available online, visited on 25-05-2025), 2016.

[23] Picoscope 4000 Series, "High-precision USB oscilloscopes," https://www.picotech.com/download/datasheets/picoscope-4000-series-data-sheet.pdf (available on line, visited on 22-05-2025), 2021.

[24] National Semiconductors, "High q notch filter," www.ti.com/lit/pdf/snoa680.pdf (available online, last access on July 11, 2025), 1969.